Chronobiology International, Early Online: 1–15, (2013)

ISSN 0742-0528 print/1525-6073 online
DOI: 10.3109/07420528.2012.754453

informa
healthcare

Effect of Experimental Diabetic Retinopathy on the Non-Image-Forming Visual System

Diego C. Fernandez,[1] Pablo H. Sande,[1] Nuria de Zavalía,[1] Nicolás Belforte,[1] Damián Dorfman,[1] Leandro P. Casiraghi,[2] Diego Golombek,[2] and Ruth E. Rosenstein[1]

[1]*Laboratorio de Neuroquímica Retiniana y Oftalmología Experimental, Departamento de Bioquímica Humana, Facultad de Medicina/CEFyBO, Universidad de Buenos Aires/CONICET, Buenos Aires, Argentina,* [2]*Laboratorio de Cronobiología, Universidad Nacional de Quilmes/CONICET, Bernal, Provincia de Buenos Aires, Argentina*

Diabetic retinopathy is a leading cause of blindness. Intrinsically photosensitive retinal ganglion cells (ipRGCs), which express the photopigment melanopsin, are involved in non-image-forming visual responses such as photoentrainment of circadian rhythms and pupilary light reflex. Since several reports indicate that retinal ganglion cells are affected by diabetes, we investigated the non-image-forming visual system in an advanced stage of experimental diabetes in rats induced by streptozotocin. After 15 wks of diabetes induction, clear alterations in the visual function were observed and all animals developed mature cataracts. At this time point, concomitantly with a significant decrease in the number of Brn3a(+) retinal ganglion cells, no differences in the number of melanopsin-containing cells, melanopsin levels, and retinal projections to the suprachiasmatic nuclei and the olivary pretectal nucleus were observed. At high light intensity, afferent pupil light reflex appears to be conserved in diabetic animals. After 15 wks of diabetes induction, a significant decrease in light-induced c-Fos expression in the suprachiasmatic nuclei was found. In diabetic animals, the locomotor activity pattern was conserved, although a delay in the time needed for re-entrainment after a phase delay was observed. In diabetic animals, lensectomy reversed the alterations in c-Fos expression and in the locomotor activity rhythm. These results suggest that the neuronal substrate of the non-image-forming visual system remained largely unaffected at advanced stages of diabetes, and that lensectomy, a relatively easy and safe surgery, could partially restore circadian alterations induced by diabetes. (Author correspondence: ruthr@fmed.uba.ar)

Keywords: Diabetic retinopathy, Lensectomy, Melanopsin, Non-image-forming visual system, Suprachiasmatic nuclei

INTRODUCTION

Diabetic retinopathy (DR), one of the most common complications of diabetes, is a leading cause of blindness in people of working age in industrialized countries, and affects the daily lives of millions of people. Although DR has long been recognized as a vascular disease, it is becoming increasingly clear that retinal cells are also affected by diabetes, resulting in dysfunction and degeneration of neuronal cells (reviewed by Kern & Barber, 2008). In a streptozotocin (STZ)-induced diabetic model in rats, we have demonstrated a significant decrease in the number of cells in the ganglion cells layer (GCL) at 15 wks after STZ injection. Moreover, we have shown axoglial alterations in the distal portion of the optic nerve that were evident even before neuron soma loss (i.e., at 6 wks of diabetes induction) (Fernandez et al., 2012).

Besides the classical photoreceptors (i.e., rods and cones), a third group of retinal photoreceptors has been identified as intrinsically photosensitive retinal ganglion cells (ipRGCs), which express the photopigment melanopsin (Berson et al., 2003; Hattar et al., 2002). These cells are responsible for conveying photic information to the brain concerning ambient illumination conditions and regulate different non-image-forming functions (e.g., synchronization of circadian clocks, pupillary light reflex [PLR]) (Lucas et al., 2003; Panda et al., 2003). Intrinsically photosensitive RGCs respond to light stimuli independently from rod and cone inputs, and send projections through the retinohypothalamic tract to the suprachiasmatic nuclei (SCN), the principal

Submitted July 17, 2012, Returned for revision August 10, 2012, Accepted November 11, 2012

Address correspondence to Dr. Ruth E. Rosenstein, Departamento de Bioquímica Humana, Facultad de Medicina, CEFyBO, Paraguay 2155, 5°P, (1121), Universidad de Buenos Aires, CONICET, Buenos Aires, Argentina. Tel.: 54-11-4508-3672 (ext. 37); Fax: 54-11-4508-3672 (ext. 31); E-mail: ruthr@fmed.uba.ar

pacemaker for circadian rhythms, and the olivary pretectal nucleus (OPN), responsible for the PLR (Hattar et al., 2006). A strong body of evidence supports that ipRGCs are involved in modulating circadian rhythms (Hattar et al., 2003; Panda et al., 2003). Considering the key role of the photic information in the generation of biological rhythms (Golombek & Rosenstein, 2010), it is of great interest to determine how ophthalmic diseases may affect the circadian timing system. It was shown that ipRGCs and RGCs, which project to the superior colliculus (SC), are similarly vulnerable to the deleterious effects of chronic ocular hypertension (Drouyer et al., 2008; de Zavalía et al., 2011). Moreover, experimental glaucoma in rats induces significant alterations in the non-image-forming visual system (de Zavalía et al., 2011). Surprisingly, taking into account the high incidence of diabetes and its influence on retinal function, and considering that normal circadian rhythms are fundamental for healthy conditions, the link between diabetes and circadian rhythms has only been addressed in a relatively limited number of studies. In that sense, some alterations of circadian rhythms were described in people with type 1 diabetes (Gallego et al., 2008; Gil et al., 2009; Jauch-Chara et al., 2008). Moreover, it has been previously shown that 2 mos after the administration of STZ to Wistar rats, the number of Fos-immunoreactive cells in the SCN decreased significantly (Yamanouchi et al., 1997), which indicates that chronic diabetic conditions may affect the light-entraining responses in the SCN. In addition, some clock genes exhibited altered expression in the liver, heart, and kidney from diabetic animals (Herichová et al., 2005; Oishi et al., 2004; Young, 2006). These findings support the idea that a critical relationship may exist between diabetes and the circadian system. The association between diabetes and the non-image-forming visual system was poorly examined, and the obtained results are relatively contradictory. Using a mouse model of diabetes (Ins2 Akita/+), Gastinger et al. (2008) reported a decrease in retinal ganglion cell (RGC) number and abnormal swelling of somas, axons, and dendrites noted in all subtypes of RGCs, including ipRGCs. In contrast, Kumar and Zhuo (2011) have shown an intense melanopsin(+) dendritic network of ipRGCs in whole-mounted retinas and increased levels of melanopsin mRNA after 4 wks of STZ injection in mice. In this context, we considered it worthwhile to analyze the non-image-forming visual system in advanced stages of experimental diabetes induced by STZ injection.

MATERIALS AND METHODS

Animals

Male Wistar rats (average weight: 300–350 g) were housed in a standard animal room with food and water ad libitum under controlled conditions of humidity and temperature (21°C ± 2°C) and under a 12-h light/12-h dark lighting schedule (lights on at 08:00 h). For diabetes induction, a single intraperitoneal injection of STZ (60 mg/kg in .1 M citrate buffer, pH 4.5) was performed. Control rats received an equal volume of citrate buffer. Animals were examined 72 h after injections using a glucose meter (Bayer Laboratories, Buenos Aires, Argentina) and those with blood glucose levels greater than 350 mg/dL were considered diabetic. Rats were monitored weekly and the body weight and plasma glucose levels were determined.

The ethics committee of the University of Buenos Aires School of Medicine, (Institutional Committee for the Care and Use of Laboratory Animals [CICUAL]) approved this study, which agrees with Association for Research in Vision and Ophthalmology, Inc. (ARVO) Statement for the Use of Animals in Ophthalmic and Vision Research. The experimental protocol conformed to international ethical standards (Portaluppi et al., 2010).

Onset and Progression of Cataract and Lensectomy

Cataract development was monitored weekly using a handheld ophthalmoscope equipped with a slit lamp. Cataract development was considered complete when the red fundus reflex was no longer visible through any part of the lens, and when the lens appeared dull white to the naked eye (Figure S1). At 11–12 wks post injection of STZ, all animals developed mature cataract.

Lensectomy

Animals were anesthetized with ketamine hydrochloride (150 mg/kg) and xylazine hydrochloride (2 mg/kg) administered intraperitoneally. Phenylephrine hydrochloride (2%) and tropicamide (.5%) were used to dilate the pupil and proparacaine was topically applied. A small incision was made in the cornea with a sharp blade and a second incision was made in the anterior lens capsule. Using fine forceps, the lens (with the anterior capsule) was carefully removed without affecting the posterior capsule. Saline solution was constantly applied. Finally, the cornea was sutured with nylon 10/0. After lensectomy, animals were treated with nepafenac .1% (Alcon Laboratories, Buenos Aires, Argentina) and moxifloxacin .5% (Alcon Laboratories) for 7 d (eye drops, twice a day). A clinical analysis was performed regularly after surgery and the visual function was evaluated 7 and 14 d after surgery (Figure 1). No differences were observed in the electroretinogram (ERG) after lensectomy. Moreover, the clinical study did not indicate signs of postsurgery ocular inflammation (Figure S1).

Electroretinography

Electroretinographic activity was assessed as previously described (Fernandez et al., 2009). Briefly, after 6 h of dark adaptation, rats were anesthetized under dim red illumination. Phenylephrine hydrochloride and tropicamide were used to dilate the pupils, and the cornea was intermittently irrigated with balanced salt solution to maintain the baseline recording and to prevent keratopathy. Rats were placed facing the stimulus at a distance of

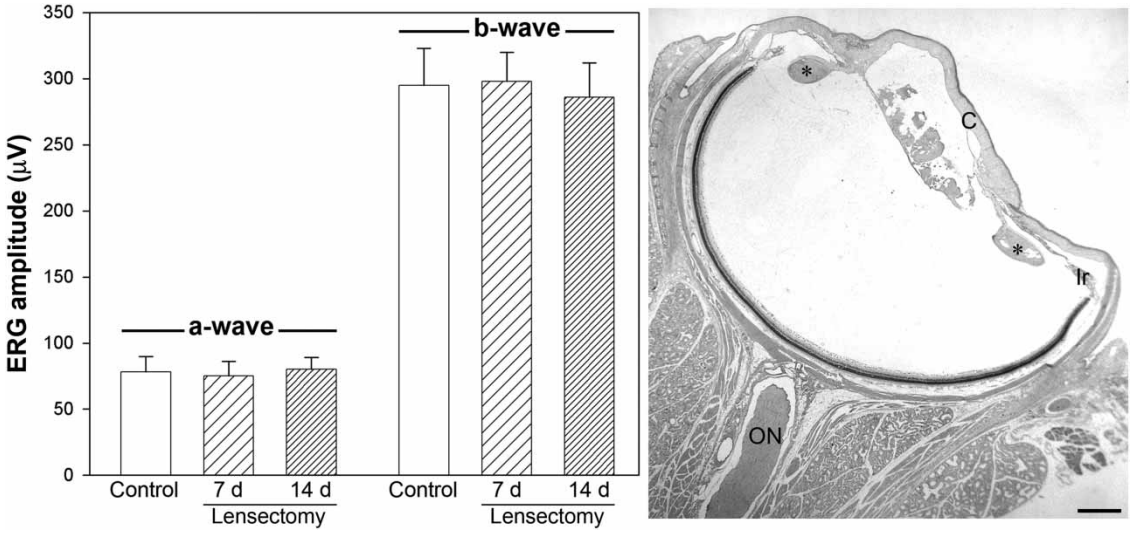

FIGURE 1. Functional and histopathological analysis following lens extraction (preserving only the posterior lens capsule) in control animals. No significant alterations in the functional responses were observed at 7 or 14 d post lensectomy. After surgery, animals were allowed to recover for 9 wks and the eyes were morphologically evaluated. In all cases, intact vitreous camera and retina were observed. No signs of lens regeneration were evident, except for small structures build up of lens-like material present only in the margin (asterisks). Scale bar = 1 mm. ON = optic nerve; C = cornea; Ir = iris.

20 cm. All recordings were completed within 20 min and animals were kept warm during and after the procedure. A reference electrode was placed through the ear, a grounding electrode was attached to the tail, and a gold electrode was placed in contact with the central cornea. A 15-W red light was used to enable accurate electrode placement. This maneuver did not significantly affect dark adaptation and was switched off during the electrophysiological recordings. Electroretinograms (ERGs) were recorded from both eyes simultaneously and 10 responses to flashes of unattenuated white light (5 ms, .2 Hz) from a full-field/Ganzfeld stimulator (light-emitting diodes) set at maximum brightness (9 cd·s/m^2 without a filter). Flash responses were amplified, filtered (1.5-Hz low-pass filter, 1000 high-pass filter, notch activated) and averaged (Akonic BIO-PC; Akonic, Buenos Aires, Argentina). The a-wave was measured as the difference in amplitude between the recording at onset and the trough of the negative deflection and the b-wave amplitude was measured from the trough of the a-wave to the peak of the b-wave. Runs were repeated 3 times with 5-min intervals to confirm consistency. Mean values from each eye were averaged, and the resultant mean value was used to compute the group mean a- and b-wave amplitudes ± SEM. The mean peak latencies and peak-to-peak amplitudes of the responses from each group of rats were compared.

Oscillatory potentials (OPs) were assessed as previously described (Fernandez et al., 2009). Briefly, the same photic stimulator with a .2-Hz frequency and filters of high (300 Hz) or low (100 Hz) frequency were used. The amplitudes of the OPs were estimated by measuring the heights from the baseline drawn between the troughs of successive wavelets to their peaks. The sum of three OPs was used for statistical analysis.

Flash Visual Evoked Potentials

Scotopic flash visual evoked potentials (VEPs) were recorded as previously described (Belforte et al., 2010). For this purpose, two stainless steel electrodes were surgically placed 4 mm lateral to the interhemispheric fissure and 5.6 mm posterior to bregma (active electrode). Reference electrodes were placed 2 mm lateral to the midline and 2 mm anterior to bregma. A ground electrode was placed in the animal tail. Both electrodes were isolated and fixed with dental acrylic and the skin was sutured with nylon 5/0. Four days after electrode implantation, VEPs were assessed as follows: after 6 h of dark adaptation, rats were anesthetized, pupils were dilated, and the cornea was intermittently irrigated as previously described, under dim red illumination. All recordings were completed within 20 min of the induction of anesthesia and animals were kept warm during and after the procedure. Each eye was recorded individually, occluding the contralateral eye with black carbon paper and cotton, and a 70-stimulus average was recorded. Eyes were stimulated with unattenuated white light (1 Hz) from a photic stimulator (light-emitting diodes) set at maximum brightness (.95 log cd·s/m^2). Flash responses were amplified, filtered (.5-Hz low-pass filter, 100 high-pass filter, notch activated), and averaged (Akonic BIO-PC; Akonic). The latency to the N2 deflection and the P2 peak was assessed.

Cholera Toxin β-Subunit Injection

Animals (5 rats/group) were anesthetized, and a drop of proparacaine (.5%) was topically administered for local anesthesia. Four microliters of a solution of .2% cholera toxin β-subunit (CTB) conjugated to Alexa 488 dye (Molecular Probes, Eugene, OR, USA) in .1 M phosphate-buffered saline (PBS; pH 7.4) were injected into

the vitreous using a 30-gauge Hamilton syringe (Hamilton, Reno, NV, USA). Injections were applied at 1 mm of the limbus and the needle was left in the eye for 1 min to prevent volume loss. At 3 d after injection, rats were anesthetized and intracardially perfused with saline solution followed by a solution containing 4% formaldehyde in .1 M PBS (pH 7.4). The brains were carefully removed and postfixed overnight at 4°C, immersed in a graded series of sucrose solutions (10%, 20%, and 30%), and coronal sections (40 μm) were obtained using a Leica CM 1850 freezing microtome (Buenos Aires, Argentina). Nuclei were stained with the fluorescent dye 4′,6-diamidino-2-phenylindole (DAPI), mounted with antifade medium (Vectashield; Vector Laboratories, Burlingame, CA, USA), and viewed with a fluorescence microscope (BX50; Olympus, Tokyo, Japan) connected to a video camera (3CCD; Sony, Tokyo, Japan) attached to a computer running image analysis software (ImagePro Plus; Media Cybernetics, Rockville, MD, USA).

For all immunofluorescence studies, comparative digital images from different samples were grabbed using identical exposition time, brightness, and contrast settings. All images were assembled and processed in Adobe Photoshop SC (Adobe Systems, San Jose, CA, USA) to adjust the brightness and contrast. No other adjustment was made. All the nomenclature used in the paper follows that of Paxinos and Watson (1997).

RGC Studies

Anesthetized rats were intracardiacally perfused as previously described. The posterior eye cups were immersed in an ice-cold fixative for 4 h. Retinas were carefully detached and flat-mounted with the vitreous side up in superfrost microscope slides (Erie Scientific, Portsmouth, NH, USA). Whole-mount retinas were preincubated with 5% normal horse serum for 1 h, and then incubated overnight at 4°C with a rabbit polyclonal anti-melanopsin (1:1000; Affinity Bioreagent, Rockford, IL, USA) and a goat polyclonal anti-Brn3a (1:500; Santa Cruz Biotechnology, Santa Cruz, CA, USA) primary antibodies. After several washings, an anti-rabbit secondary antibody conjugated to Alexa Fluor 488 (1:1000; Molecular Probes) and an anti-goat secondary antibody conjugated to Alexa Fluor 568 (1:500; Molecular Probes) were added, and sections were incubated for 2 h at room temperature. Regularly, some sections were treated without the primary antibodies to confirm specificity. After immunostaining, nuclei were stained with DAPI and viewed with a fluorescence microscope as previously described.

For all morphometric image processing and analysis, digitalized captured TIFF images were transferred to ImageJ software (National Institutes of Health, Bethesda, MD, USA). To determine the number of RGC Brn3a(+), the retina was divided in four quadrants, and images from the central and peripheral areas were obtained. The number of neurons was calculated in a square area corresponding to 1 mm^2. Images were converted to 8-bits gray scale and a manual threshold value, first determined by visual examination, was constantly applied. For each image, the number of cells was quantified and results obtained from each quadrant were averaged and recorded as the representative value for each retina. For each group, the mean of 5 eyes was recorded as the representative value.

The total number of melanopsin(+) cells per retina was determined. For each retina, photomicrographs were obtained separately at low magnification; the complete retina was digitally reconstructed, and the cells were manually counted. Finally, a schematic drawing of the immunostained retinas was obtained. For each group, the mean of 5 eyes was recorded as the representative value.

Western Blotting

Retinas were homogenized in 150 μL of a buffer containing 10 mM HEPES, 1 mM EDTA, 1 mM EGTA, 10 mM KCl, Triton .5% (*v*/*v*), pH 7.9, supplemented with a cocktail of protease inhibitors (Sigma Chemical, St Louis, MO, USA). After 15 min at 4°C, homogenates were gently vortexed for 15 s and centrifuged at 3000 × *g* for 10 min. Supernatants were used to determine protein concentration. Proteins (50 μg/sample) were separated in 12% sodium dodecyl sulfate polyacrylamide gel electrophoresis (SDS-PAGE). After electrophoresis, proteins were transferred to polyvinylidene difluoride membranes for 60 min at 15 V in a Bio-Rad Trans-Blot SD system (Bio-Rad Laboratories, Hercules, CA, USA). Membranes were blocked in 5% nonfat dry milk in Tris-buffered saline (pH 7.4) containing .1% Tween-20 for 60 min at room temperature and then incubated overnight at 4°C with a rabbit polyclonal anti-melanopsin antibody (1:1000). Membranes were washed and then incubated for 1 h with a horseradish peroxidase–conjugated secondary antibody. Immunoblots were visualized by enhanced chemiluminescence Western blotting detection reagents (Amersham Biosciences, Buenos Aires, Argentina). Autoradiographical signals were quantified by densitometry using ImageQuant software and adjusted by the density of β-actin. Protein content was determined by the method of Lowry et al. (1951), using bovine serum albumin as the standard.

Assessment of Light-Induced c-Fos Expression in the SCN

Animals were subjected to a 1-h light stimulus (1200 lux) 4 h after turning off the lights (i.e., at 00.00 h; zeitgeber time [ZT] 16). Then, rats were kept under darkness for 30 min and were anesthetized and perfused (under darkness) as previously described. Some animals were kept constantly under darkness until sacrifice. Brains were postfixed overnight in the same fixative. Coronal sections (40 μm) were obtained using a freezing microtome, collected in .1 M PBS and washed with .4% Triton X-100 in .0 1 M PBS (PBS-t). Sections were preincubated with 2% normal horse serum and .4% Triton X-100 in .1 M PBS for 1 h, treated with .3% H_2O_2 in PBS for 20 min

(for blocking endogenous peroxidase activity), and incubated for 72 h at 4°C with a rabbit polyclonal antibody anti-c-Fos (1:5000; Santa Cruz Biotechnology). The immunohistochemical detection was performed using the LSAB2 System-HRP (Dako, Carpinteria, CA, USA), based on biotin-streptavidin-peroxidase, and visualized using 3,3'-diaminobenzidine (DAB) as chromogen. Serial sections were analyzed and the total number of c-Fos(+) neurons in the retinoreceptive area of the SCN were counted. For each group, the mean of 6 nuclei was recorded as the representative value.

Assessment of the Pupil Light Reflex

Animals were dark-adapted for 2 h prior to PLR assessment. While one eye received light stimulation from a white light source (1200, 500, or 180 lux), the other eye was video-monitored under infrared light with a digital camcorder (Sony DCR-SR60; Tokyo, Japan). Sampling rate was 30 images per second. The digital video recording was deconstructed to individual frames using OSS Video Decompiler Software (One Stop Soft, New England, USA). The percent pupil constriction was calculated as the percent of pupil area at 30 s after the initiation of the stimulus (steady state) relative to the dilated pupil size. For each group, the mean of 10 eyes was recorded as the representative value.

Locomotor Activity Rhythm

Circadian rhythms of locomotor activity were recorded in control and diabetic animals, under 12-h light (200 lux)/12-h dark cycles. Rats were placed in cages equipped with infrared detectors of motion, data were sampled every 5 min and stored for subsequent analysis. Double-plot actograms, periodograms, and average activity waveforms were built with El Temps software (A. Díez-Noguera, Barcelona, Spain). The phase angle for activity onset (with respect to the time of lights off) was determined, defined as the first of 5-min activity bins in which locomotor activity was higher than the average value of the diurnal waveform. In addition, the percentage of locomotor activity during the light and dark phases was computed.

Re-entrainment rates were calculated after 4 h of phase delay in the light-dark (L:D) cycle, starting by shifting the time for lights off. The sigmoidal curve-fitting were obtained using the Microcal Origin Software (Microcal Software, Northampton, MA, USA).

Statistical Analysis

Statistical analysis of results was made by a Student's *t* test or a two-way analysis of variance (ANOVA) followed by Dunnett's test or Tukey's test, as stated.

RESULTS

Table 1 summarizes the average body weight and blood glucose levels after the injection of vehicle or STZ. A significant body weight loss and an increase in blood glucose levels were observed in STZ-treated rats as compared with vehicle-injected rats.

Experimental diabetes induced significant alterations of the visual function, as shown in Figure 2. At 10 wks of diabetes induction, a significant decrease in the ERG a- and b-wave amplitudes (Figure 2A–B) and in the sum of OP amplitudes (Figure 2C) was observed. No significant progression of the visual dysfunction was observed at 12 or 15 wks of diabetes. In addition, a significant increase in the VEP N2 and P2 pick latencies was observed after 12 and 15 wks of diabetes induction (Figure 2D). With the progression of diabetes, all animals developed cataracts that were clearly evident from wks 11 to 12 after STZ injection. In order to evaluate the involvement of lens opacity in the ERG and VEPs, a bilateral lensectomy was performed in a group of animals after 6 wks of diabetes induction. Animals were allowed to recover for 9 wks after surgery, and a functional and histopathological analysis was performed at 15 wks post injection of STZ. No significant differences in ERG, OPs, and VEPs were observed between diabetic animals without or with lensectomy (Figure 2A–D). As in control animals (Figure 1), no signs of retinal alterations were observed in eyes from diabetic animals submitted to lensectomy (Figure S1).

The active anterograde transport of RGC projections to the main retinorecipient targets in the brain was analyzed using CTB, as shown in Figure 3. In control animals, a strong CTB-staining was observed in the superficial layers of the SC, the SCN, and the OPN. After 6, 10, or 15 wks of diabetes induction, a clear reduction in the CTB-staining was observed in the SC, extending in

TABLE 1. Average body weight and blood glucose concentration assessed at different time points

	Average of body weight (g)		Average of blood glucoseconcentration (mg/dL)	
Time after vehicle or STZ injection	Control	Diabetes	Control	Diabetes
3 d	338.5 ± 12.4	330.9 ± 14.4	101.2 ± 5.7	420.3 ± 27.2**
6 wks	452.5 ± 11.7	324.7 ± 13.1**	104.8 ± 6.9	499.2 ± 17.7**
10 wks	473.9 ± 13.8	319.9 ± 12.8**	107.5 ± 10.2	542.3 ± 13.7**
15 wks	489.4 ± 16.5	312.2 ± 14.7**	113.5 ± 11.4	564.8 ± 16.1**

A significant decrease in body weight and an increase in blood glucose levels were observed after STZ injection. Data are mean ± SEM (n = 10 animals/group). **$p < .01$ vs. aged-matched control animals, by Dunett's test.

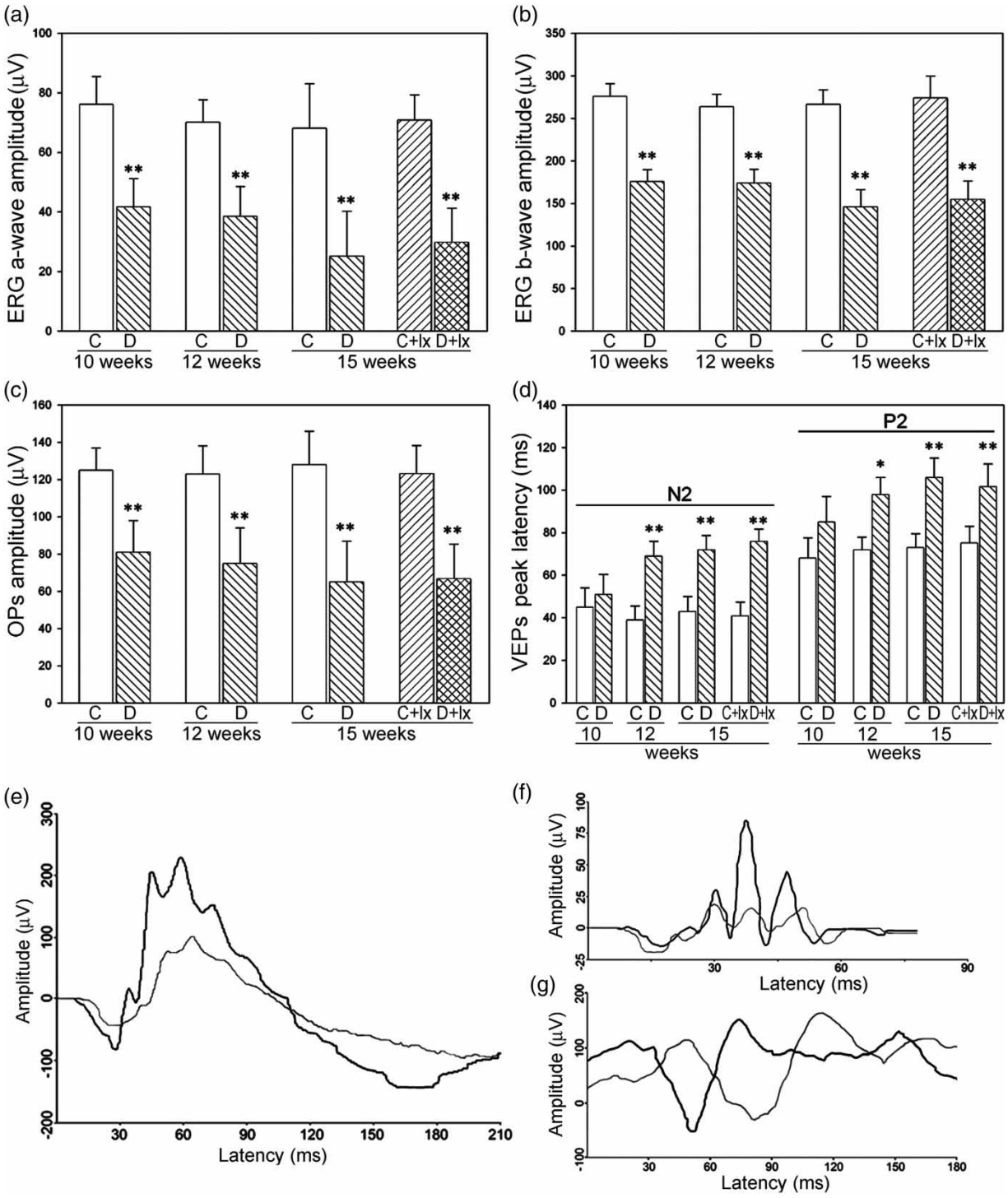

FIGURE 2. Effect of experimental diabetes on retinal and visual pathway function. After 10 wks of diabetes induction a significant decreased in the ERG a-wave (A) and b-wave (B) amplitudes as well as in the sum of OP amplitude (C) was observed, without clear signs of progression of the dysfunction. In another group of animals submitted to bilateral lensectomy after 6 wks of diabetes induction, no differences were observed in ERG or OP responses evaluated at 15 wks after STZ injection. (D) The VEP analysis revealed a significant increase in N2-P2 pick latencies after 12 and 15 wks of diabetes induction (with or without lensectomy), as compared with age-matched control animals. (E–G) Representative ERG, OP, and VEP traces from a control animal (black trace) and an animal after 15 wks of STZ injection (gray trace). Data are the mean ± SEM (n = 10 animals per group); $^{*}p < .05$, $^{**}p < .01$ vs. age-matched controls, by Tukey's test. C, control; D = diabetes; C + lx = control + lensectomy; D + lx = diabetes + lensectomy.

rostral to caudal direction. However, a preserved pattern of CTB-staining was observed in the SCN as well as in the OPN from diabetic animals. Figure 3 shows representative photomicrographs obtained from serial coronal sections through the entire SC, SCN, and OPN of an age-matched control and a 15-wk diabetic animal. Lensectomy in diabetic animals did not modify the CTB-staining pattern in retinorecipient areas (SC, SCN,

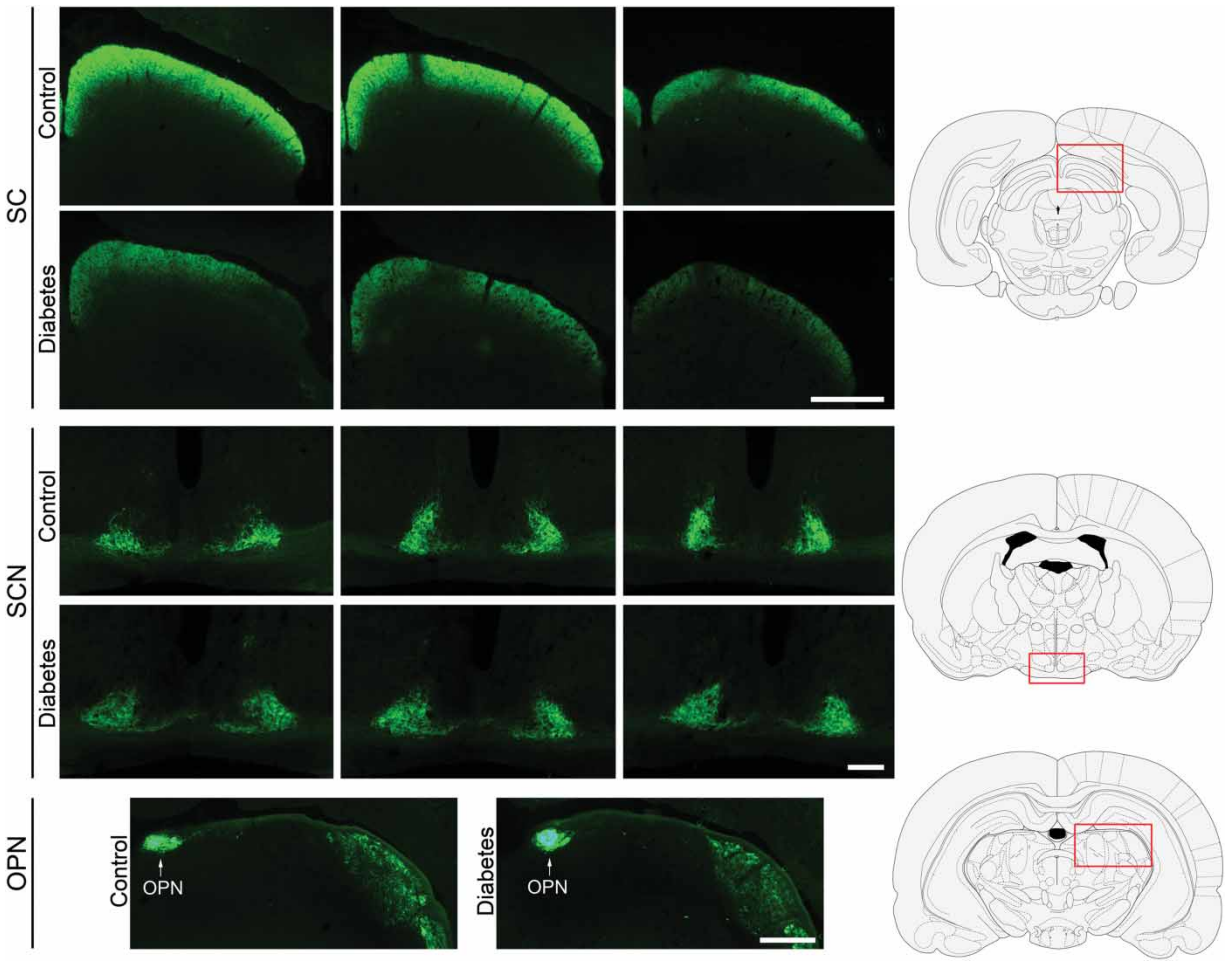

FIGURE 3. CTB-staining pattern in the SC, SCN, and OPN. Upper panel: Representative photomicrographs of coronal sections (rostral, medial, and caudal portions) of the SC from a control and a 15-wk diabetic animal. After 15 wks of diabetes induction, a clear reduction of the retinal terminal field density in the SC was observed, as compared with control animals. Middle and lower panels: No signs of alterations in the CTB-staining were observed in serial sections obtained at the SCN or the OPN level between groups. The zone of interest is represented in red boxes in the right panel. Scale bar: upper panel = 1 mm; middle panel = 200 μm; lower panel = 500 μm. Shown are photomicrographs representative of 5 animals/group.

and OPN) as compared with diabetic eyes without lensectomy (Figure S2).

In animals that were diabetic for 15 wks, a significant decrease in the number of Brn3a(+) cells was observed in flat-mounted retinas, as compared with the control group (Figure 4A–C), particularly in retinal periphery. In order to determine the influence of experimental diabetes on ipRGCs, the presence of melanopsin(+) cells was analyzed by immunofluorescence. An intense labeling of cell bodies and dendrites that overlapped extensively and form a reticular network was observed in control and diabetic rats (Figure 4A–B). No differences in the total number of melanopsin(+) neurons were found between nondiabetic animals and animals that were diabetic for 15 wks (Figure 4D–F). The number of Brn3a(+) (in the central and peripheral retina) and melanopsin(+) cells did not differ between diabetic eyes without or with lensectomy (Figure S3).

In order to further analyze the effect of diabetes on melanopsin, the protein levels were assessed by Western blotting. After 15 wks of diabetes, no changes in melanopsin levels were detected as compared with age-matched controls (Figure 4G–H).

The PLR was examined at 10 wks of diabetes induction. It was not possible to assess the PLR at longer times of diabetes because of cataract development. When eyes were stimulated with intense light (1200 lux), no differences in maximal pupil constriction were observed among groups. However, under less intense light (500 or 180 lux), a slight but significant decrease in the PLR was observed in diabetic eyes (Figure 5).

The functional connectivity between RGCs and the SCN was examined by measuring light-induced c-Fos expression in neurons from the ventrolateral part of the SCN. For this purpose, a light pulse (1 h; 1200 lux) was applied at 00.00 h (4 h after lights off, ZT 16) in control and diabetic animals. In 15-wk diabetic animals, a significant decrease in the total number of c-Fos(+) cells in the SCN were observed (Figure 6). In another set of 6-wk diabetic animals, the lens was surgically removed, and the same stimulation protocol was applied after 15 wks of

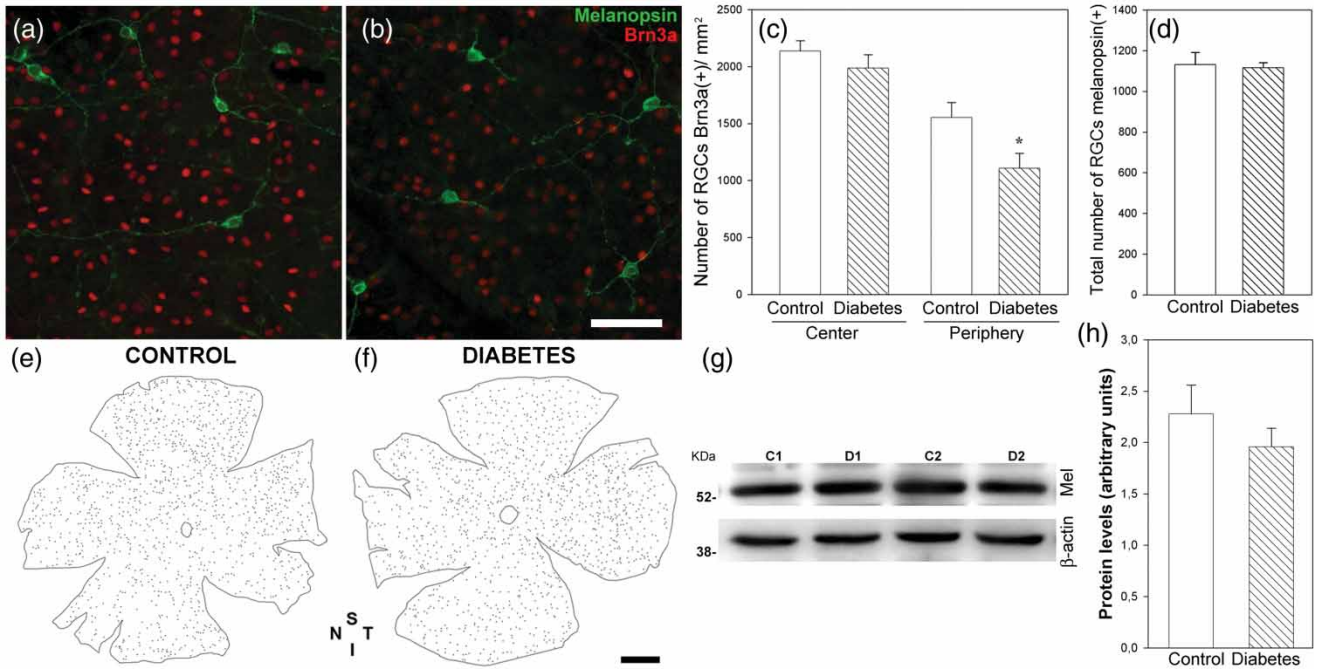

FIGURE 4. RGC analysis and melanopsin levels in advanced stages of diabetes. (A, B) Representative photomicrographs of double immunostaining for Brn3a (red) and melanopsin (green) cells in flat-mounted retinas from a control and a 15-wk diabetic animal. (C) Quantification of Brn3a(+) cells. A significant decrease in the number of Brn3a(+) cells was observed in diabetic animals. (D) The total number of melanopsin(+) cells was evaluated per retina in flat-mounted preparations. No differences were observed between groups. (E, F) Representative diagrams showing the total number of melanopsin(+) cells per retina. (G) Retinal melanopsin levels assessed by Western blotting in control and 15-wk diabetic animals. Shown are representative Western blots with samples from controls (C1, C2) and 15-wk diabetic animals (D1, D2). (H) Densitometric analysis of all samples. No changes in melanopsin levels were observed between groups. Data are the mean ± SEM (n = 5 retinas/group). *$p < .05$ vs. age-matched control, by Student's t test. Scale bar = 100 μm (B); 25 μm (F). N = nasal; T = temporal; S = superior; I = inferior.

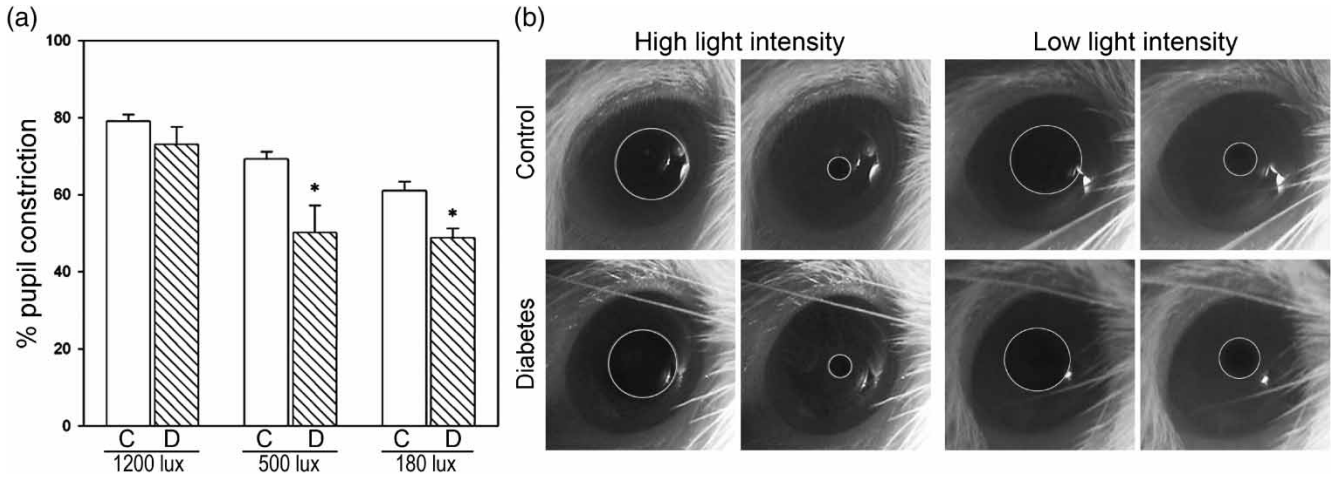

FIGURE 5. Assessment of the consensual PLR in control and 10-wk diabetic animals. (A) The pupil diameter (relative to the limbus diameter) was measured before and after a photic stimulus (white light, 1200, 500, or 180 lux) and the percentage of pupil constriction was calculated. At 1200 lux, no significant differences were observed among groups, whereas at 500 and 180 lux a slight but significant decrease in the PRL was observed in diabetic animals. Representative images of the PRL from a control and a 10-wk diabetic animal exposed to 1200 lux (left) or 180 lux (right) are shown in panel B. Data are the mean ± SEM (n = 10 animals/group). *$p < .05$ vs. age-matched control, by Student's t test.

STZ injection. Lensectomy, which showed no effect per se in control animals, significantly prevented the diabetes-induced decrease in c-Fos(+) neuron number (Figure 6).

The locomotor activity rhythm and the response to a phase shift in the L:D cycle were measured in control and diabetic animals. The locomotor activity pattern in diabetic animals from wks 10 to 15 after STZ injection

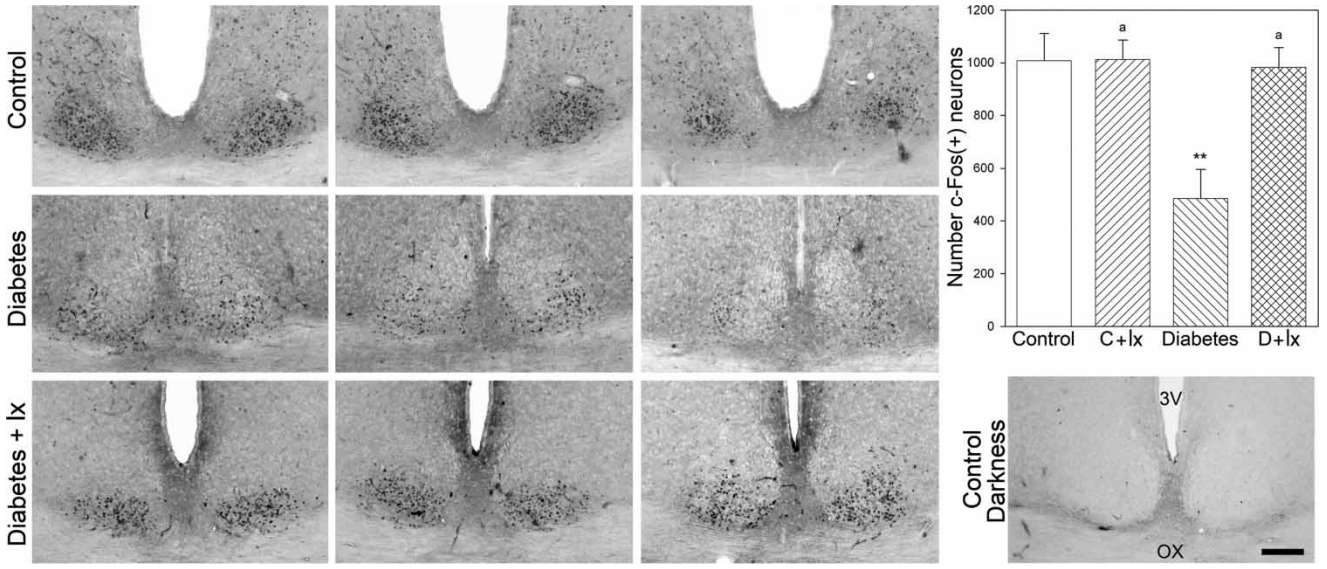

FIGURE 6. Light-induced c-Fos expression in the SCN. Animals were exposed to a white light pulse (1200 lux) for 1 h at ZT 16 (4 h after lights off). The total number of c-Fos(+) immunoreactive neurons was quantified in serial coronal sections from control and 15-wk diabetes animals without or with lensectomy performed at 6 wks after STZ injection. Shown are three representative photomicrographs (rostral, medial, and caudal portions of the retinotopic SCN) from different groups. A control darkness is also shown. Diabetes induced a significant decrease in the number of c-Fos(+) neurons in the SCN compared with age-matched controls, which was completely reversed by lensectomy. Data are the mean ± SEM (n = 5 animals/group). $^{**}p < .01$ vs. age-matched control, $^{a}p < .01$ vs. 15-wk diabetes without lensectomy, by Tukey's test. Scale bar = 200 μm. C + lx = control + lensectomy; D + lx = diabetes + lensectomy; 3V = third ventricle; OX = optic chiasm.

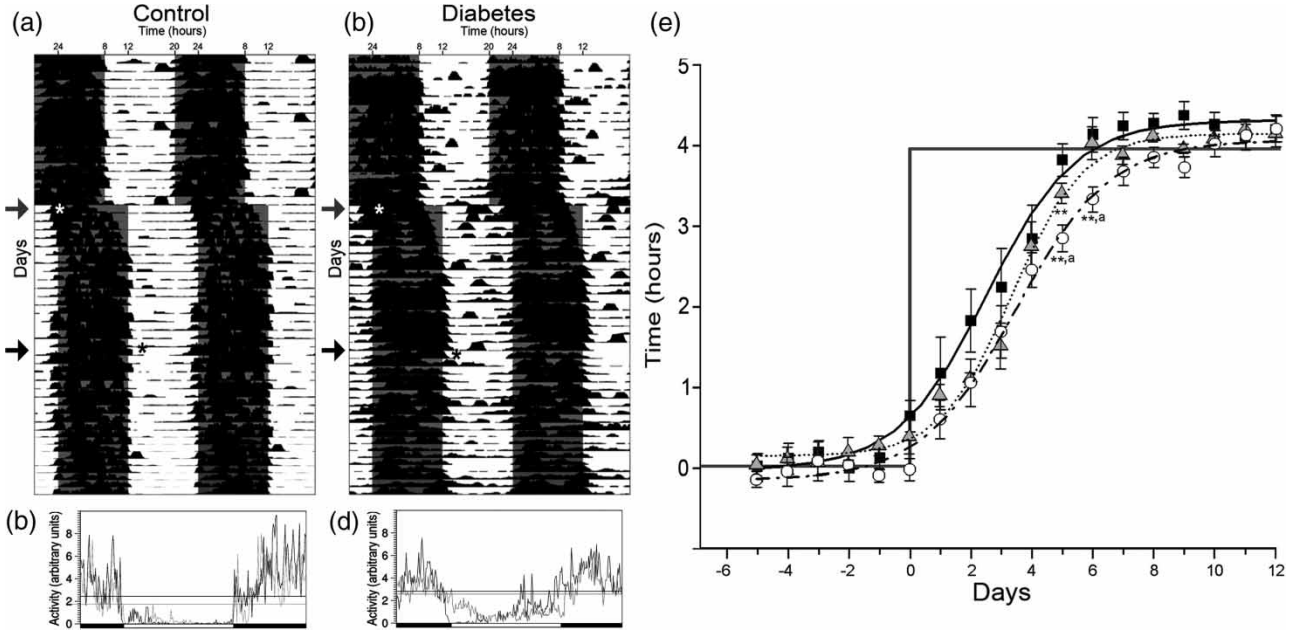

FIGURE 7. Locomotor activity rhythm from control, diabetic animals, and diabetic animals submitted to lensectomy. (A, B) Double-plotted actograms of a representative control or a diabetic rat under a normal L:D cycle. A 4-h phase delay in the L:D cycle was applied (gray arrows and white asterisks) and the period needed for re-entrain was evaluated. Finally, animals were submitted to bilateral lensectomy (black arrows and black asterisks) and alterations in the activity rhythm pattern were evaluated. (C, D) Representative waveforms from a control and a diabetic animal before (black trace) and after (grey trace) lensectomy. (E) Time for re-entrainment after a 4 h-phase delay in the L:D cycle evaluated in control (black dots), and 15-wk diabetic animals without (white circles) or with lensectomy (gray triangles). The *y*-axis shows the progression in time for activity onset after the change in the L:D cycle. A sigmoidal curve-fitting was applied (Control [continuous line]: $R^2 = .989$; Diabetes [dashed line]: $R^2 = .992$; Diabetes + lensectomy [dotted line]: $R^2 = .980$). A significant increase in the time needed to re-entrain the locomotor activity rhythm was observed in diabetic animals compared with control rats. This alteration was partially reversed by lensectomy. Data are the mean ± SEM (n = 6 animals/group). $^{**}p < .01$ vs. age-matched control; $^{a}p < .01$ vs. 15-wk diabetic animals, by Tukey's test.

revealed a normal rhythm of activity entrained to a L:D cycle (Figure 7A–D). However, a significant delayed phase angle of activity onset with respect to the time of lights off was observed in diabetic animals. The phase angle was 3.4 ± 3.1 and 29.13 ± 6.4 min for control and diabetic animals, respectively (n = 10; $p < .01$, Student's t test). In addition, the percentage of locomotor activity in the photophase was significantly higher in diabetic than in control rats (control: 10.0% ± 2.5% vs. diabetes: 28.9% ± 2.3%; $p < .01$, Student's t test). To evaluate the influence of lens opacity on these alterations, a bilateral lensectomy was performed in 15-wk diabetic animals. After 15 d of recovery, the re-entrainment rate to a normal L:D cycle was evaluated. A similar locomotor activity profile was observed in diabetic lensectomized animals as compared with results from diabetic animals before surgery (Figure 7A–D). In this group, the phase angle was 30.0 ± 1.4 min and the percentage of locomotor activity in the photophase was 27.1% ± 1.1%. After a 4-h phase delay of the L:D cycle, a significant increase in the time needed to re-entrain the locomotor activity rhythm was observed in diabetic animals, as shown in Figure 7E (control: 4.8 ± .3 d vs. diabetes: 7.3 ± .2 d; $p < .01$, Student's t test). However, in diabetic animals submitted to lensectomy, a partial but significant prevention of the increase in this parameter was observed (diabetes + lensectomy: 5.8 ± .3 d; $p < .05$ vs. control, $p < .01$ vs. diabetes without lensectomy, Student's t test).

DISCUSSION

The present results indicate a general preservation of the non-image-forming system at advanced stages of experimental diabetes (i.e., at 15 wks post injection of STZ). At this time point, alterations in the retina-SC connection, a significant decrease in retinal (ERG) and optic pathway (VEP) function, and in Brn3a(+) RGC number was evident, whereas melanopsin(+) cell number, melanopsin levels, and the retina-SCN and the retina-OPN connections were preserved.

CTB is a reliable anterograde tracer that is taken up by RGC bodies in the retina and transported to the tips of axons (Angelucci et al., 1996; Prichard et al., 2007). As previously shown (Fernandez et al., 2012), the present results confirmed a deficit in the CTB anterograde transport from the retina to the SC (its primary projection site) in advanced stages of diabetes, whereas no evident changes were observed in CTB anterograde transport from the retina to the SCN and OPN. Since it was demonstrated that the majority of SCN- and OPN-projecting RGCs are melanopsin-immunopositive (Chen et al., 2011; Gooley et al., 2003; Hattar et al., 2006), these results suggest a preferential ipRGC axon protection in experimental diabetes. The underlying mechanism for the resistance of ipRGC axons to diabetic injury is uncertain. Based on the conduction velocity (~3 m/s), Trejo and Cicerone (1984) have suggested that axons that innervate the OPN correspond to small diameter fibers. Recently, we have shown that STZ-induced diabetes provokes damage to large axons, whereas small axons are spared, at least at early stages of diabetes (Fernandez et al., 2012). Therefore, differences in axon diameter could account for the particular preservation of ipRGC axons. Moreover, the preservation was observed not only at axonal level, but also at ipRGC somas. Brn3a is a POU domain transcription factor that is specifically expressed in RGC nuclei (Nadal-Nicolás et al., 2009). Although Brn3a was considered a marker for the total population of RGCs, it was recently demonstrated that the subpopulation of ipRGCs is Brn3a(–) (Jain et al., 2012). As shown herein, a significant decrease in Brn3a (+) cell number occurred in advanced stages of diabetes, whereas no changes in melanopsin(+) cell number were evident. This result was supported by the assessment of melanopsin levels, which remained unchanged after 15 wks of diabetes.

Notably, it was recently reported that ipRGCs resist neurodegeneration in two inherited mitochondrial disorders that cause blindness, i.e., Leber hereditary optic neuropathy and dominant optic atrophy (La Morgia et al., 2011), but not in another blinding disorder characterized by extensive and selective loss of RGCs, such as glaucoma (de Zavalía et al., 2011; Drouyer et al., 2008). In addition, other evidences of ipRGCs robustness are provided by studies on cell toxicity to glutamate (Chambille & Serviere, 1993; Hannibal et al., 2001). The underlying mechanism for the ipRGC resistance to diabetic injury is uncertain. The phylogenetic origin of ipRGCs is very ancient and relates to invertebrate rhabdomeric photoreception, which predates the development of the eye as the organ for vision (Peirson et al., 2009). Thus, a long-lasting evolutionary pressure conserved this photoreceptive system, possibly selecting its intrinsic robustness (Hannibal et al., 2001). We do not know at this stage whether the neural circuit within the retina or the unique functionalities of this group of cells associated with this photopigment contributes to the survival after injury, but these issues will be examined in the near future.

In addition to the soma and axon preservation, the present results support that the functionality of ipRGCs is also considerably preserved in advanced stages of diabetes. Historically, it was assumed that the light evoked neural signals driving the PLR originated exclusively from rods and cones. However, later on, it was shown that ipRGCs significantly contribute to the maintenance of pupil constriction (Lucas et al., 2003). The current view is that pupil responses differ as a function of light intensity and wavelength, and that selected stimulus conditions can produce pupil responses that reflect phototransduction primarily mediated by rods, cones, or melanopsin. In this vein, it is accepted that responses driven by melanopsin occur at higher levels of illumination than those driven by classical photoreceptors, and conversely, at lower light intensity, cones and rods would be involved in PRL changes (Lucas et al., 2003;

Grozdanic et al., 2007). At 10 wks of diabetes, no differences in the PLR were observed as compared with nondiabetic animals when eyes were stimulated with high-intensity light, whereas at lower intensities, a decrease in the PRL was observed in diabetic eyes, which is compatible with a photoreceptor-deficient activity shown by the decrease in the ERG induced by experimental diabetes. The iris is innervated by terminals from neurons located in the Edinger-Westphal nuclei that receives terminals from the OPN. After 15 wks of diabetes induction, no signs of alterations in the CTB-staining pattern in the OPN were observed. These results suggest a functional and morphological preservation of the connection between the retina and the OPN in advanced stages of diabetes.

The discovery of ipRGCs came from the observation that mice with extensive degeneration of rods and cones, such as homozygous (rd/rd) mice lacking rods or mice lacking all functional rod and cone photoreceptors (rd/rd cl), were still capable of normal circadian photoentrainment (Foster et al., 1991; Lucas et al., 1999) and PLR (Lucas et al., 2001). In agreement with other authors (Hancock & Kraft, 2004; Shinoda et al., 2007), experimental diabetes induced significant alterations in the scotopic ERG. The a-wave of the flash ERG is classically thought to represent photoreceptor activity, whereas the b-wave reflects bipolar and Müller cell function. The present results strongly support that experimental diabetes induced a functional impairment of the inner and outer retina. Thus, STZ-induced diabetes could be a suitable and biologically meaningful model to analyze ipRGC functions in a background of a marked alteration of the outer and inner retina function, as shown by the significant decrease in scotopic ERG a- and b-wave and OP amplitudes in diabetic animals. In that sense, concomitantly with a significant decrease in the electroretinographic activity, a clear preservation of the PLR was observed in diabetic eyes, which further supports that melanopsin could be necessary and sufficient for this nonvisual photoresponse.

The assessment of light-induced c-Fos expression is a useful tool for measuring the functional connectivity between the retina and the SCN. The proto-oncogene c-Fos is a transcription factor that regulates several target genes (Morgan & Curran, 1991). Moreover, it was demonstrated that intracerebroventricular injections of antisense oligonucleotides that inhibit Fos expression block the light-induced phase shifts of the activity rhythm (Wollnik et al., 1995). Yamanouchi et al. (1997) showed that 2 mos after the administration of STZ to Wistar rats, the number of Fos-immunoreactive cells significantly decreases in the SCN after a light stimulus. In agreement, the present results further support a decrease in light-induced c-Fos expression in the SCN at 15 wks of diabetes. Since cataract is a usual complication of diabetes, it seems possible that lens opacity may account for the decrease in the photic input from the retina to the SCN. To test this hypothesis, animals were lensectomized at 6 wks of diabetes, and light-induced c-Fos expression was assessed at 15 wks post injection of STZ. Lensectomy, which showed no effect per se on retinal function in control or diabetic animals, prevented the effect of diabetes on light-induced c-Fos expression in the SCN, supporting that cataract may be responsible for the alteration of this parameter in diabetic animals. In lensectomized diabetic animals, light-induced c-Fos expression in the SCN was indistinguishable from that observed in nondiabetic animals, suggesting that experimental diabetes did not affect the light-induced neuronal activation of the SCN and, presumably, the photic response of the mammalian circadian clock. To analyze this hypothesis, we recorded general activity patterns for both control and 15-wk diabetic animals. Notably, despite the fact that 15-wk diabetic animals were considerably sick, diabetic rats exhibited normal circadian rhythms under a light-dark cycle. However, subtle changes indicated that entrainment in diabetic animals is somewhat impaired. In that sense, diabetic animals were significantly more active during the photophase than nondiabetic animals, suggesting a decreased mechanism of photic entrainment. In addition, since diabetes likely increases the need to drink, this effect could account for the increased daytime activity. A significant change in the phase angle for the start of their nocturnal locomotion was also observed in diabetic animals. This could be interpreted either as a deficient fine-tuning for photic entrainment, as a lack of the masking response to lights off, or both. Interestingly, the waveform analysis of locomotor activity in control rats showed a clear masking of this rhythm, indicated by the sharp increase and decrease of locomotion around the times of transition of the L:D cycle. This marked masking was not observed in the waveforms corresponding to diabetic animals, which show a less pronounced transition in locomotor patterns during light and dark conditions. Also in this case, it is also possible that general bad conditions of diabetic animals affect the activity rhythm. Both entrainment and masking to light contribute to normal synchronization of rhythms, and both mechanisms depend on an intact circadian photoreception pathway (Golombek & Rosenstein, 2010). In agreement with Shimazoe et al. (2000), we also observed alterations in the re-entrainment rate of locomotor activity rhythm after a phase delay of the L:D cycle, which was partially reversed by lensectomy. These general differences in entrainment might represent an impaired phototransduction mechanism in the retinohypothalamic tract that would translate into a deficient communication between the retinal and the SCN clocks. However, no morphological or functional alterations were observed in the diabetic retinohypothalamic pathway. In that sense, Shimazoe et al. (2000) demonstrated that after 8 wks of diabetes, the level of phase delay induced by glutamate application in the SCN neuronal firing rhythm was similar to that observed in control samples.

Significant alterations in activity rhythms and sleep architecture, as well as in cognitive tasks, were described in patients with lens opacity (Brøndsted et al., 2011; Kessel et al., 2011; Schmoll et al., 2011). Our results demonstrate that alterations in the non-image-forming system in diabetic animals could be mainly attributed to cataract, as shown by the fact that lensectomy significantly prevented the effect of diabetes. In agreement, Kessel et al. (2010) have postulated that lens opacity reduces light input, affecting particularly the blue spectrum, and in consequence, the photic input to ipRGCs.

Circadian rhythm disorders may include sleep problems, impaired performance, decrease in cognitive skills, poor psychomotor coordination, and headaches, among many others, which can significantly worsen the quality of life of diabetic patients. The present results suggest that the neuronal substrate of the non-image-forming visual system remained largely unaffected at advanced stages of diabetes, and that lensectomy, a relatively easy and safe surgery in humans, could restore circadian alterations induced by diabetes.

Declaration of Interest: This research was supported by grants from the Agencia Nacional de Promoción Científica y Tecnológica (PICT 1623); The University of Buenos Aires (M062); and CONICET (PIP 1911), Argentina. The funding organizations have no role in the design or conduct of this research.

The authors report no conflicts of interest. The authors alone are responsible for the content and writing of the paper.

REFERENCES

Angelucci A, Clascá F, Sur M. (1996). Anterograde axonal tracing with the subunit B of cholera toxin: a highly sensitive immunohistochemical protocol for revealing fine axonal morphology in adult and neonatal brains. *J. Neurosci. Methods* 65:101–112.

Belforte N, Sande P, de Zavalía N, Knepper PA, Rosenstein RE. (2010). Effect of chondroitin sulfate on intraocular pressure in rats. *Invest. Ophthalmol. Vis. Sci.* 51:5768–5775.

Berson DM, Dunn FA, Takao M. (2002). Phototransduction by retinal ganglion cells that set the circadian clock. *Science* 295:1070–1073.

Brøndsted AE, Lundeman JH, Kessel L. (2013). Short wavelength light filtering by the natural human lens and IOLs —implications for entrainment of circadian rhythm. *Acta Ophthalmol.* 91:52–57.

Chambille I, Serviere J. (1993). Neurotoxic effects of neonatal injections of monosodium L-glutamate (L-MSG) on the retinal ganglion cell layer of the golden hamster: anatomical and functional consequences on the circadian system. *J. Comp. Nerurol.* 338:67–82.

Chen SK, Badea TC, Hattar S. (2011). Photoentrainment and pupillary light reflex are mediated by distinct populations of ipRGCs. *Nature* 476:92–95.

de Zavalía N, Plano SA, Fernandez DC, Lanzani MF, Salido E, Belforte N, Sarmiento MI, Golombek DA, Rosenstein RE. (2011). Effect of experimental glaucoma on the non-image forming visual system. *J. Neurochem.* 117:904–914.

Drouyer E, Dkhissi-Benyahya O, Chiquet C, WoldeMussie E, Ruiz G, Wheeler LA, Denis P, Cooper HM. (2008). Glaucoma alters the circadian timing system. *PLoS ONE* 3:e3931.

Fernandez DC, Chianelli MS, Rosenstein RE. (2009). Involvement of glutamate in retinal protection against ischemia/reperfusion damage induced by post-conditioning. *J. Neurochem.* 111:488–498.

Fernandez DC, Pasquini LA, Dorfman D, Aldana Marcos HJ, Rosenstein RE. (2012). Early distal axonopathy of the visual pathway in experimental diabetes. *Am. J. Pathol.* 180:303–313.

Foster RG, Provencio I, Hudson D, Fiske S, De Grip W, Menaker M. (1991). Circadian photoreception in the retinally degenerate mouse (rd/rd). *J. Comp. Physiol.* 169A:39–50.

Gallego PH, Craig ME, Hing S, Donaghue KC. (2008). Role of blood pressure in development of early retinopathy in adolescents with type 1 diabetes: prospective cohort study. *BMJ* 337:a918.

Gastinger MJ, Kunselman AR, Conboy EE, Bronson SK, Barber AJ. (2008). Dendrite remodeling and other abnormalities in the retinal ganglion cells of Ins2 Akita diabetic mice. *Invest. Ophthalmol. Vis. Sci.* 49:2635–2642.

Gill GV, Woodward A, Casson IF, Weston PJ. (2009). Cardiac arrhythmia and nocturnal hypoglycaemia in type 1 diabetes—the 'dead in bed' syndrome revisited. *Diabetologia* 52:42–45.

Golombek DA, Rosenstein RE. (2010). Physiology of circadian entrainment. *Physiol. Rev.* 90:1063–1102.

Gooley JJ, Lu J, Fischer D, Saper CB. (2003). A broad role for melanopsin in nonvisual photoreception. *J. Neurosci.* 23:7093–7106.

Grozdanic SD, Matic M, Sakaguchi DS, Kardon RH. (2007). Evaluation of retinal status using chromatic pupil light reflex activity in healthy and diseased canine eyes. *Invest. Ophthalmol. Vis. Sci.* 48:5178–5183.

Hancock HA, Kraft TW. (2004). Oscillatory potential analysis and ERGs of normal and diabetic rats. *Invest. Ophthalmol. Vis. Sci.* 45:1002–1008.

Hannibal J, Vrang N, Card JP, Fahrenkrug J. (2001). Light-dependent induction of cFos during subjective day and night in PACAP-containing ganglion cells of the retinohypothalamic tract. *J. Biol. Rhythms* 16:457–470.

Hattar S, Liao HW, Takao M, Berson DM, Yau KW. (2002). Melanopsin-containing retinal ganglion cells: architecture, projections, and intrinsic photosensitivity. *Science* 295:1065–1070.

Hattar S, Lucas RJ, Mrosovsky N, Thompson S, Douglas RH, Hankins MW, Lem J, Biel M, Hofmann F, Foster RG, Yau KW. (2003). Melanopsin and rod-cone photoreceptive systems account for all major accessory visual functions in mice. *Nature* 424:76–81.

Hattar S, Kumar M, Park A, Tong P, Tung J, Yau KW, Berson DM. (2006). Central projections of melanopsin-expressing retinal ganglion cells in the mouse. *J. Comp. Neurol.* 497:326–349.

Herichová I, Zeman M, Stebelová K, Ravingerová T. (2005). Effect of streptozotocin-induced diabetes on daily expression of per2 and dbp in the heart and liver and melatonin rhythm in the pineal gland of Wistar rat. *Mol. Cell. Biochem.* 270:223–229.

Jain V, Ravindran E, Dhingra NK. (2012). Differential expression of Brn3 transcription factors in intrinsically photosensitive retinal ganglion cells in mouse. *J. Comp. Neurol.* 520:742–755.

Jauch-Chara K, Schmid SM, Hallschmid M, Born J, Schultes B. (2008). Altered neuroendocrine sleep architecture in patients with type 1 diabetes. *Diabetes Care* 31:1183–1188.

Kern TS, Barber AJ. (2008). Retinal ganglion cells in diabetes. J. Physiol. 586:4401–4408.

Kessel L, Lundeman JH, Herbst K, Andersen TV, Larsen M. (2010). Age-related changes in the transmission properties of the human lens and their relevance to circadian entrainment. *J. Cataract Refract. Surg.* 36:308–312.

Kessel L, Siganos G, Jørgensen T, Larsen M. (2011). Sleep disturbances are related to decreased transmission of blue light to the retina caused by lens yellowing. *Sleep* 34:1215–1219.

Kumar S, Zhuo L. (2011). Quantitative analysis of pupillary light reflex by real-time autofluorescent imaging in a diabetic mouse model. *Exp. Eye Res.* 92:164–172.

La Morgia C, Ross-Cisneros FN, Hannibal J, Montagna P, Sadun AA, Carelli V. (2011). Melanopsin-expressing retinal ganglion cells: implications for human diseases. *Vision Res.* 51:296–302.

Lowry OH, Rosebrough NJ, Farr AL, Randall RJ. (1951). Protein measurement with the Folin Phenol reagent. *J. Biol. Chem.* 193:265–275.

Lucas RJ, Freedman MS, Munoz M, Garcia-Fernandez JM, Foster RG. (1999). Regulation of the mammalian pineal by non-rod, non-cone, ocular photoreceptors. *Science* 284:505–507.

Lucas RJ, Douglas RH, Foster RG. (2001). Characterization of an ocular photopigment capable of driving pupillary constriction in mice. *Nat. Neurosci.* 4:621–626.

Lucas RJ, Hattar S, Takao M, Berson DM, Foster RG, Yau KW. (2003). Diminished pupillary light reflex at high irradiances in melanopsin-knockout mice. *Science* 299:245–247.

Morgan JL, Curran T. (1991). Stimulus-transcription coupling in the nervous system: involvement of the inductible proto-oncogenes fos and jun. *Annu. Rev. Physiol.* 14:421–445.

Nadal-Nicolás FM, Jiménez-López M, Sobrado-Calvo P, Nieto-López L, Cánovas-Martínez I, Salinas-Navarro M, Vidal-Sanz M, Agudo M. (2009). Brn3a as a marker of retinal ganglion cells: qualitative and quantitative time course studies in naive and optic nerve-injured retinas. *Invest. Ophthalmol. Vis. Sci.* 50:3860–3868.

Oishi K, Kasamatsu M, Ishida N. (2004). Gene- and tissue-specific alterations of circadian clock gene expression in streptozotocin-induced diabetic mice under restricted feeding. *Biochem. Biophys. Res. Commun.* 317:330–334.

Panda S, Provencio I, Tu DC, Pires SS, Rollag MD, Castrucci AM, Pletcher MT, Sato TK, Wiltshire T, Andahazy M, Kay SA, Van Gelder RN, Hogenesch JB. (2003). Melanopsin is required for non-image-forming photic responses in blind mice. *Science* 301:525–527.

Paxinos G, Watson C. (1997). *The rat brain in stereotaxic coordinates.* Amsterdam: Elsevier, 125 pp

Peirson SN, Halford S, Foster RG. (2009). The evolution of irradiance detection: melanopsin and the non-visual opsins. *Philos. Trans. R. Soc. Lond. B Biol. Sci.* 364:2849–2865.

Portaluppi F, Smolensky MH, Touitou Y. (2010). Ethics and methods for biological rhythm research on animals and human beings. *Chronobiol. Int.* 27:1911–1929.

Prichard JR, Armacanqui HS, Benca RM, Behan M. (2007). Light-dependent retinal innervation of the rat superior colliculus. *Anat. Rec. (Hoboken)* 290:341–348.

Schmoll C, Tendo C, Aspinall P, Dhillon B. (2011). Reaction time as a measure of enhanced blue-light mediated cognitive function following cataract surgery. *Br. J. Ophthalmol.* 95:1656–1659.

Shimazoe T, Ishida J, Maetani M, Yakabe T, Yamaguchi M, Miyasaka K, Kono A, Watanabe S, Funakoshi A. (2000). Entrainment function in the suprachiasmatic nucleus of streptozotocin-induced diabetic rats. *Jpn. J. Pharmacol.* 83:355–358.

Shinoda K, Rejdak R, Schuettauf F, Blatsios G, Völker M, Tanimoto N, Olcay T, Gekeler F, Lehaci C, Naskar R, Zagorski Z, Zrenner E. (2007). Early electroretinographic features of streptozotocin-induced diabetic retinopathy. *Clin. Exp. Ophthalmol.* 35:847–854.

Trejo LJ, Cicerone CM. (1984). Cells in the pretectal olivary nucleus are in the pathway for the direct light reflex of the pupil in the rat. *Brain Res.* 300:49–62.

Wollnik F, Brysch W, Uhlmann E, Gillardon F, Bravo R, Zimmermann M, Schlingensiepen KH, Herdegen T. (1995). Block of c-Fos and JunB expression by antisense oligonucleotides inhibits light-induced phase shifts of the mammalian circadian clock. *Eur. J. Neurosci.* 7:388–393.

Yamanouchi S, Shimazoe T, Nagata S, Moriya T, Maetani M, Shibata S, Watanabe S, Miyasaka K, Kono A, Funakoshi A. (1997). Decreased level of light-induced Fos expression in the suprachiasmatic nucleus of diabetic rats. *Neurosci. Lett.* 227:103–106.

Young ME. (2006). The circadian clock within the heart: potential influence on myocardial gene expression, metabolism, and function. *Am. J. Physiol. Heart Circ. Physiol.* 290:H1–H16.

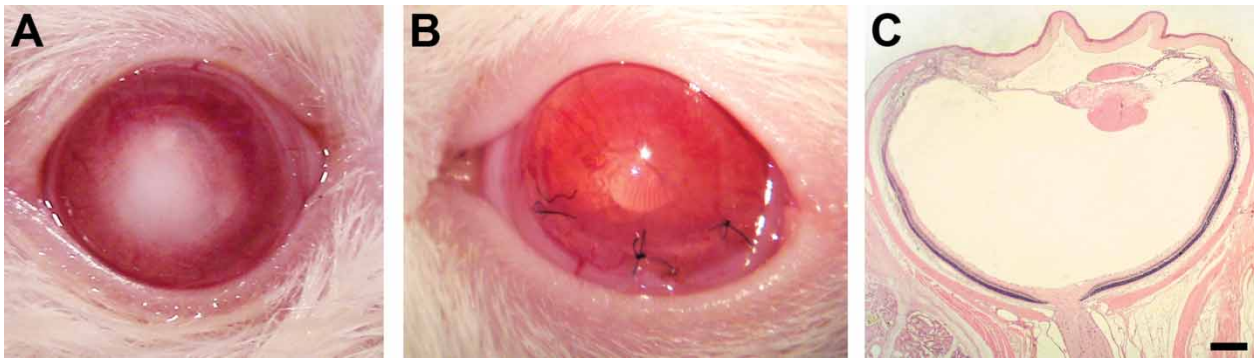

FIGURE S1. Histopathological analysis following lens extraction (preserving only the posterior lens capsule) in diabetic animals. After 11–12 wks, most diabetic animals developed lens opacity (A). Diabetic animals were submitted to lensectomy, and a clinical (B) and a morphological (C) analysis were performed at 7 d and 9 wk post surgery, respectively. (C) Scale bar = 1 mm.

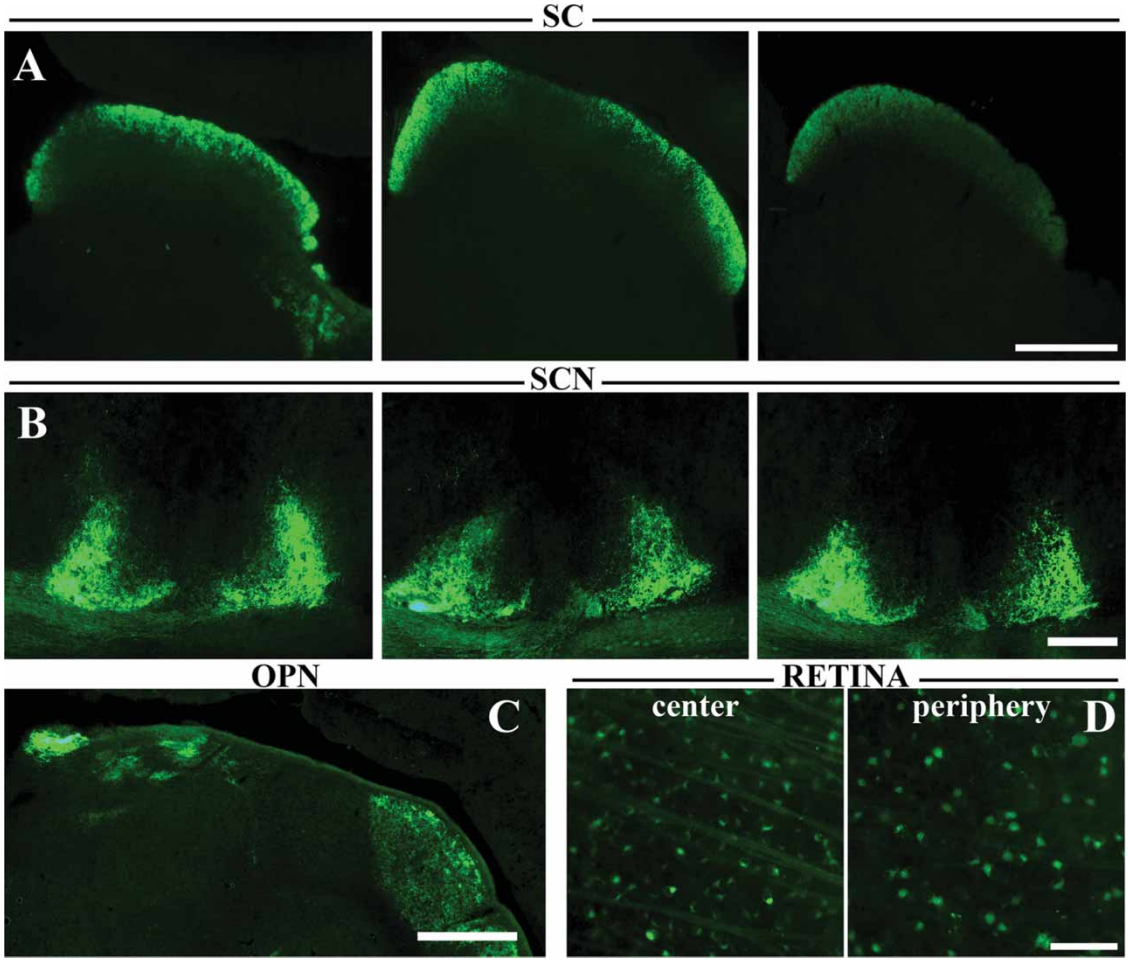

FIGURE S2. CTB-staining pattern in the SC, SCN, and OPN in 15-wk diabetic animals submitted to lensectomy. (A) Representative photomicrographs of coronal sections (rostral, medial, and caudal portions) of the SC. A clear reduction of the retinal terminal field density in the SC was observed. No signs of alterations in the CTB-staining were observed in serial sections through the entire SCN (B) or the OPN (C). (D) As a control of injection, most retinal cells showed extensive CTB uptake. Scale bar = 1 mm (A); 200 μm (B); 500 μm (C); 100 μm (D). Shown are photomicrographs representative of 4 animals.

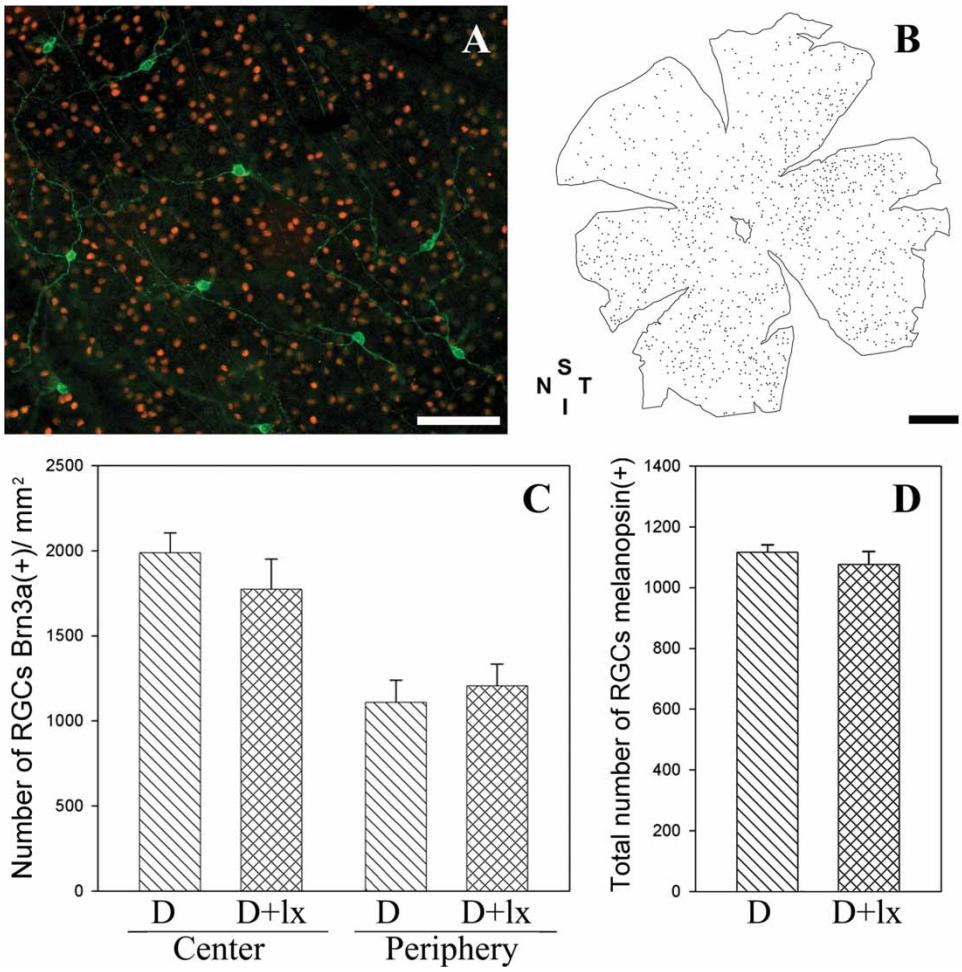

FIGURE S3. RGC analysis in 15-wk diabetic animals submitted to lensectomy. (A) Representative photomicrograph of double immunostaining for Brn3a (red) and melanopsin (green) cells in flat-mounted retinas. (B) The total number of melanopsin(+) cells per retina was evaluated in flat-mounted preparations. Quantification of Brn3a(+) (C) and melanopsin(+) (D) cells revealed no differences between 15-wk diabetic animals with or without lensectomy. Data are the mean ± SEM (n = 4–5 retinas/group). Scale bar = 100 μm (A); 25 μm (F). N = nasal; T = temporal; S = superior; I = inferior; D = diabetes; D + lx = diabetes + lensectomy.